

# Di-photon rate enhancement in the NMSSM with nearly degenerate scalar and pseudoscalar Higgs bosons

Shoaib Munir, Leszek Roszkowski\*, Sebastian Trojanowski  
National Centre for Nuclear Research, Hoża 69, 00-681 Warsaw, Poland

Shoaib.Munir@fuw.edu.pl,  
L.Roszkowski@sheffield.ac.uk,  
Sebastian.Trojanowski@fuw.edu.pl

May 6, 2013

## Abstract

We propose a scenario in the Next-to-Minimal Supersymmetric Standard Model in which its both lightest scalar and pseudoscalar Higgs bosons have masses around 125 GeV. The pseudoscalar can produce an enhanced  $\gamma\gamma$  decay rate due to light higgsino-like charginos in its effective one-loop coupling to two photons. In that case, it should contribute to the  $\gamma\gamma$  rate measured at the LHC, but not to the  $WW/ZZ$  decay modes. Thus a discrepancy should be observed between the rates in these two decay channels through precise measurements. However, the pseudoscalar will stay hidden behind the SM-like scalar Higgs boson in the dominant gluon fusion production mode and in order for it to be observable the  $b\bar{b}h$  production mode has to be considered. We analyze the constrained NMSSM with non-universal Higgs sector parameters, and identify regions in its parameter space where the lightest pseudoscalar with mass around 125 GeV and a measurable  $\gamma\gamma$  rate in the  $b\bar{b}h$  mode can be obtained.

## 1 Introduction

Since its observation at the LHC in July 2012 [1, 2], the CMS and ATLAS collaborations have accumulated more data and updated their results on the Higgs boson. In the early results, a considerable enhancement in the  $\gamma\gamma$  and  $ZZ$  rates compared to the Standard Model (SM) prediction was noted near  $\sim 125$  GeV at the ATLAS detector. According to the CMS data, the signal strength,  $\sigma/\sigma_{\text{SM}}$ , was consistent with the SM prediction in the  $ZZ$  channel but an enhancement in the  $\gamma\gamma$  channel was observed there as well. However, the figures from both experiments have changed in the latest results released after the collection of  $\sim 20/\text{fb}$  of data [3, 4]. The signal strengths measured by the CMS have now fallen down to SM-like values in the  $\gamma\gamma$  and  $ZZ$  decay channels with the mean value of the boson mass being  $125.6 \pm 0.64$  GeV. The ATLAS collaboration, on the other hand, still reports significant excesses,  $\sigma/\sigma_{\text{SM}} = 1.65 \pm 0.35$  in the  $\gamma\gamma$  channel with the mass measurement yielding  $126.8 \pm 0.73$  GeV, and  $\sigma/\sigma_{\text{SM}} = 1.7 \pm 0.5$  in the  $ZZ$  channel with mass at  $124.3^{+0.55}_{-0.4}$  GeV. Moreover, broad peaks consistent with a 125 GeV boson have now also been observed in the  $H \rightarrow WW \rightarrow 2l2\nu$  channel at the two detectors. Importantly, the best-fit signal

---

\*On leave of absence from the University of Sheffield, UK.

strength in this channel is very SM-like according to both CMS and ATLAS, with a measured value of  $0.76 \pm 0.21$  at the former and of  $1.01 \pm 0.31$  at the latter.

Since the first announcements of the discovery of the boson, there have been many attempts to interpret the observed data in light of various supersymmetric (SUSY) extensions of the SM [5, 6, 7, 8, 9, 10, 11, 12, 13, 14, 15]. In the context of the Minimal Supersymmetric Standard Model (MSSM) the observed signal can be interpreted as being due to the lightest Higgs boson of the model,  $h$ . In the MSSM constrained at the grand unification theory (GUT) scale, referred to as the CMSSM [16],  $h$  can attain a mass around the measured central value only if the SUSY-breaking scale,  $M_{\text{SUSY}}$ , is much larger than 1 TeV, while also satisfying other important phenomenological constraints. In the Next-to-Minimal Supersymmetric Standard Model (NMSSM) [17, 18] (see, e.g., [19, 20] for a review) it has been shown that either of the two lightest CP-even Higgs bosons,  $h_1$  and  $h_2$ , can easily be SM-like with mass around 125 GeV [21, 11]. In fact in this model it is possible to have  $h_1$  and  $h_2$  almost degenerate in mass around 125 GeV [9], so that the observed signal is actually a superposition of two individual peaks due to each of these, which cannot be independently resolved.

In the GUT-constrained version of the NMSSM (CNMSSM) [18, 22, 23, 24], in analogy with the CMSSM, it has been found that in order to obtain  $h_1$  as heavy as 125 GeV,  $M_{\text{SUSY}}$  at or above 1 TeV is needed even with relevant phenomenological constraints imposed [14]. Alternatively, a SM-like  $h_2$  with mass  $\sim 125$  GeV is easily achievable [14]. Relaxing slightly the universality conditions by disunifying the masses of the scalar Higgs doublets  $m_{H_u}$  and  $m_{H_d}$  from the scalar mass parameter  $m_0$  and the soft Higgs trilinear coupling parameters  $A_\lambda$  and  $A_\kappa$  from the unified soft Yukawa coupling  $A_0$ , makes it relatively easy to obtain SM-like  $h_1$  or  $h_2$  around 125 GeV [25]. Here we refer to such a model with non-universal Higgs sector parameters as CNMSSM-NUHM. The scenario with mass degenerate  $h_1$  and  $h_2$  satisfying also other phenomenological constraints has also been pursued with much interest in the CNMSSM-NUHM [9, 10].

Even though the latest results from CMS seem to favor a SM-like Higgs boson, those from ATLAS do so only partially and it is still possible for the observed boson to be a non-standard one. The inconsistencies between the various measurements and fluctuations in the data leave ample room for speculation in this regard. Therefore, in this article, we propose a scenario, not investigated hitherto, in which the lightest pseudoscalar of the model,  $a_1$ , is almost degenerate in mass with the lightest  $\sim 125$  GeV scalar,  $h_1$ . Such  $a_1$  will thus be partially responsible for an enhanced signal rate in the  $\gamma\gamma$  channel but, being a pseudoscalar, will not contribute to the  $WW$  and  $ZZ$  channels:

$$R_{\gamma\gamma}^Y(\text{obs}) \equiv \frac{\sigma_{h_i}^Y}{\sigma_{\text{SM}}^Y} = R_{\gamma\gamma}^Y(h_1) + R_{\gamma\gamma}^Y(a_1) \simeq 1 + R_{\gamma\gamma}^Y(a_1) \quad \text{and} \quad R_{WW/ZZ}^Y(\text{obs}) = R_{WW/ZZ}^Y(h_1) \simeq 1. \quad (1)$$

In the above equation the signal rate is defined as

$$R_{\gamma\gamma}^Y(h_i) = \frac{\sigma(Y \rightarrow h_i)}{\sigma(Y \rightarrow h_{\text{SM}})} \times \frac{BR(h_i \rightarrow X)}{BR(h_{\text{SM}} \rightarrow X)}, \quad (2)$$

where  $X = \gamma\gamma, ZZ/WW$  and  $h_{\text{SM}}$  is a SM Higgs boson with the same mass as  $h_i$ .  $Y$  implies the various possible Higgs production modes at the LHC, which include gluon fusion ( $ggh$ ), vector boson fusion (VBF), Higgs-strahlung off a vector boson ( $Wh/Zh$ )<sup>1</sup> and associated production off a heavy quark ( $t\bar{t}h/b\bar{b}h$ ). Our proposed solution is made possible by the contribution of a light higgsino-like chargino,  $\chi_1^\pm$ , to the effective couplings of  $a_1$  to a  $\gamma\gamma$  pair.  $h_1$  is still SM-like in this scenario due to a significant singlet component even though  $\tan\beta$  can take fairly large values [26]. Since this

---

<sup>1</sup>We note here that the VBF and  $Wh/Zh$  production modes are irrelevant for a pseudoscalar Higgs boson.

scenario is compatible with a SM-like scalar Higgs boson, it is not in conflict with the recent CMS measurements in the  $ZZ$  mode [27, 28] which disfavor the pure pseudoscalar hypothesis.

We stress that in our scenario the enhancement in the  $\gamma\gamma$  rate due to the  $a_1$  contribution will not be visible in the  $ggh$  production mode. The reason is that the small enhancement achievable in  $\frac{BR(a_1 \rightarrow X)}{BR(h_{SM} \rightarrow X)}$  ratio will be negligible in this production mode due to the very small effective coupling of the pseudoscalar to gluons which is dominated by the top quark loop. Such an enhancement can, therefore, only be noticeable in the  $b\bar{b}h$  production mode which will also get enhanced proportionally to the  $b\bar{b}$  decay width of  $a_1$ . For this reason we shall investigate this particular mode of Higgs production here. We emphasize the fact that a measurement of the signal rate due to the  $b\bar{b}h$  production channel,  $R_{\gamma\gamma}^{bb}$ , which is extremely subdominant for a SM Higgs and is therefore generally ignored, becomes enhanced by  $\tan^2 \beta$  in SUSY models and could lead to a very clear signature of our proposed scenario. Furthermore, a difference of the mass measurements in the  $\gamma\gamma$  and  $ZZ$  modes would also provide a hint for mass degenerate  $h_1$  and  $a_1$ . Such a degeneracy would imply that the signal observed in the  $\gamma\gamma$  channel should in fact be interpreted as the ‘sum’ of two individual peaks due to  $h_1$  and  $a_1$ , while the peaks in the  $ZZ/WW$  modes are because of  $h_1$  alone.

We explore regions of the CMSSM-NUHM parameter space favoring such a scenario, expecting that a discrepancy between  $\gamma\gamma$  and  $WW/ZZ$  rates will be seen by CMS and ATLAS collaborations with a focussed analysis of the  $b\bar{b}h$  production mode. We investigate the impact of other important experimental constraints on the regions of the model parameter space accommodating this scenario. They include the limits from direct SUSY searches released by ATLAS with  $\sim 20/\text{fb}$  of data as well as from the dark matter (DM) relic density measurements. We also require the corresponding parameter space to satisfy the recently announced positive  $BR(B_s \rightarrow \mu^+ \mu^-)$  measurement from the LHCb collaboration.

The article is organized as follows. In Sec. 2 we discuss the possibility of observing an enhancement in the  $\gamma\gamma$  rate at the LHC due to a  $\sim 125 \text{ GeV}$  pseudoscalar Higgs. In Sec. 3 we outline the model parameter space. In Sec. 4 we describe the experimental constraints applied in our scans, present our numerical results and discuss their salient features. We summarize our findings in Sec. 5.

## 2 Enhancement in the observed $\gamma\gamma$ rate due to a light pseudoscalar

In this section we present some analytical details of our proposed NMSSM scenario in which the correlation between the  $\gamma\gamma$  and  $WW/ZZ$  rates can be altered. One way to achieve this is with mass degenerate lightest doublet-like scalar Higgs,  $h_1$ , and lightest singlet-like pseudoscalar,  $a_1$ .

### 2.1 The pseudoscalar mass

We first discuss the conditions that are necessary to obtain a  $\sim 125$  singlet-like  $a_1$  which couples to two photons through loops of fermions and charginos only. Starting from the  $2 \times 2$  pseudoscalar mass matrix (after rotating away the Goldstone mode) [19], one can obtain the approximate expression,

$$m_{a_1}^2 \simeq -3\kappa s A_\kappa^{\text{SUSY}} - \frac{M_{P,12}^4}{M_{P,11}^2}. \quad (3)$$

In the above equation  $M_{P,12}^2 \simeq \lambda(A_\lambda^{\text{SUSY}} - 2\kappa s)v$  is the off-diagonal entry of the pseudoscalar mass matrix, where  $v \equiv \sqrt{v_u^2 + v_d^2} \simeq 174 \text{ GeV}$ , with  $v_u$  and  $v_d$  being the vacuum expectation values (vevs) of the  $u$ -type and  $d$ -type Higgs doublets, respectively, and  $A_{\lambda/\kappa}^{\text{SUSY}}$  denoting  $A_{\lambda/\kappa}$  at  $M_{\text{SUSY}}$ .

$M_{P,11}^2 \simeq \mu_{\text{eff}} B_{\text{eff}} \tan \beta$ , with  $\mu_{\text{eff}} \equiv \lambda s$  ( $s$  being the vev of the singlet field  $S$ ),  $B_{\text{eff}} \equiv A_\lambda^{\text{SUSY}} + \kappa s$  and  $\tan \beta \equiv v_u/v_d$ , is the diagonal term corresponding to the mass-squared of the doublet-like heavy pseudoscalar,  $a_2$ . The leading term in eq. (3) implies that, for positive  $\kappa$ , which we will assume here, the condition of the positivity of  $m_{a_1}^2$  depends predominantly on the relative signs of  $\mu_{\text{eff}}$  and  $A_\kappa$ . We explain the effects of negative and positive  $\mu_{\text{eff}}$  in the following.

For  $\mu_{\text{eff}} < 0$  (and therefore negative  $s$ , assuming positive  $\lambda$ ), the first term in eq. (3) is positive if  $A_\kappa > 0$  at  $M_{\text{SUSY}}$ . The second term then gives a negative correction to  $m_{a_1}^2$  depending on the sizes of  $M_{P,12}^4$ , which is positive definite, and  $M_{P,11}^2$ , which must be positive for a non-tachyonic  $a_2$ , requiring in turn  $B_{\text{eff}} < 0$ . Assuming that the correct  $m_{a_1}$  is achieved by adjusting the free parameters in the leading term, the negative contribution from the second term should be kept close to zero. This would require  $M_{P,11}^2 \gtrsim M_{P,12}^4$ . For given  $\tan \beta$  and  $\mu_{\text{eff}}$ ,  $M_{P,11}^2$  is driven by the magnitude of  $B_{\text{eff}}$ , in order to enhance which  $A_\lambda$  (which is bounded from above by  $\kappa|s|$ ) should take smaller values. However,  $A_\lambda$  at  $M_{\text{SUSY}}$  runs upwards from its GUT value with falling negative  $A_0$  owing to the contribution from relevant term in its renormalization group equation (RGE) [19]. Hence increasing negative  $A_0$  diminishes the difference between the two terms in  $B_{\text{eff}}$ , reducing its size and in turn driving  $M_{P,11}^2$  closer to zero. At the same time  $M_{P,12}$ , which is a sum of  $2\kappa|s|$  and  $A_\lambda$ , grows as  $A_\lambda$  increases, as opposed to  $M_{P,11}^2$ . Consequently, the ratio  $\frac{M_{P,12}^4}{M_{P,11}^2}$  in eq. (3) grows with decreasing  $A_0$  and, for large negative values of the latter, can result in negative  $m_{a_1}^2$ . Note also that the running of  $A_\kappa$  in turn depends dominantly on  $A_\lambda$ .  $A_\kappa$  runs upwards with  $A_\lambda$  as long as the latter is negative. When  $A_\lambda$  turns positive  $A_\kappa$  runs in the opposite direction, owing to its RGE. Thus  $A_\kappa$  in the leading term in eq. (3) will have somewhat constrained GUT scale values that can yield correct  $m_{a_1}$ . On the other hand, for  $\mu_{\text{eff}} > 0$ , the two terms in  $B_{\text{eff}}$  are both positive and the cancellation described above does not occur.

In summary, the net effect of the interplay between various Higgs sector parameters is that for negative  $\mu_{\text{eff}}$  the values of  $A_0$  at the GUT scale are bounded from below by the condition of the physicality of  $a_1$ . This constraint on  $A_0$  causes a slight tension between  $m_{h_1}$  and  $m_{a_1}$ , since it is well known that to obtain  $h_1$  which is SM-like with mass  $\sim 125$  GeV large negative values of  $A_0$  are required for  $M_{\text{SUSY}} \sim 1$  TeV. For positive  $\mu_{\text{eff}}$  there is no such tension because  $A_0$  is relatively free to take values that give large negative  $A_t$  at  $M_{\text{SUSY}}$ , as long as the correct  $a_1$  mass can be achieved by adjusting other free parameters.

## 2.2 $\gamma\gamma$ decay of the pseudoscalar

Besides a singlet-like  $a_1$  with mass similar to that of the experimentally observed boson, this scenario also requires a low mass,  $m_{\chi_1^\pm}$ , of the lightest chargino. The effective coupling of a pseudoscalar  $a_i$ , with  $i = 1, 2$ , to two photons (see, e.g., [29, 30]), is dominated by such a light chargino in the loops and can, therefore, be approximated by

$$C_{a_i}^{\text{eff}}(\gamma\gamma) \simeq \frac{g_{a_1\chi_1^\pm\chi_1^\pm}}{\sqrt{\sqrt{2}G_F} m_{\chi_1^\pm}} A_{1/2}^{a_i}(\tau_i), \quad (4)$$

where  $\tau_i = \frac{m_{a_i}^2}{4m_{\chi_1^\pm}^2}$ . For  $\tau_i \leq 1$ , which is applicable here, with  $m_{a_i} \simeq 126$  GeV and the light chargino obeying the lower limit,  $m_{\chi_1^\pm} > 94$  GeV [31], the form-factor  $A_{1/2}^{a_i}(\tau_i) = \frac{1}{\tau_i} \arcsin^2 \sqrt{\tau_i}$  [32] in the above equation lies in the range

$$1 < A_{1/2}^{a_i}(\tau_i) \lesssim 1.2. \quad (5)$$

The coupling of  $a_i$  to charginos in eq. (4) can be written, following the notation of [19], as

$$g_{a_i \chi_1^\pm \chi_1^\pm} = i \left[ \frac{\lambda}{\sqrt{2}} P_{i3} \sin \theta_U \sin \theta_V - \frac{g_2}{\sqrt{2}} (P_{i2} \cos \theta_U \sin \theta_V + P_{i1} \sin \theta_U \cos \theta_V) \right], \quad (6)$$

where  $\theta_U, \theta_V$  are the mixing angles for rotating the chargino interaction states to mass eigenstates, and  $P_{ij}$  are the entries of the mixing matrix that diagonalizes the pseudoscalar mass matrix. When the pseudoscalar weak eigenstates  $A_i^{\text{weak}}$  are expressed in the basis  $(H_{dI}, H_{uI}, S_I)$  [19],  $P_{i1}$  corresponds to  $H_{dI}$ ,  $P_{i2}$  to  $H_{uI}$  and  $P_{i3}$  to  $S_I$ .

The first term in eq. (6) implies that  $\sin \theta_{U,V} \simeq 1$  (yielding a higgsino-like  $\chi_1^\pm$ ),  $P_{13} \simeq 1$  and that larger values of  $\lambda$  are needed in order to enhance  $C_{a_1}^{\text{eff}}(\gamma\gamma)$  for the singlet-like  $a_1$ . Under these conditions, the coupling of  $a_1$  to  $b\bar{b}$  is naturally suppressed due to the tiny  $H_{dI}$  component. On the other hand, for the doublet-like pseudoscalar,  $a_2$ , an enhancement in  $C_{a_2}^{\text{eff}}(\gamma\gamma)$  requires either  $\cos \theta_U \sin \theta_V$  or  $\sin \theta_U \cos \theta_V$  to be non-negligible. This can be realized only in a very limited region of the parameter space where  $M_2 \simeq \mu_{\text{eff}}$  and not too large in order to keep  $m_{\chi_1^\pm}$  low. Moreover, in such a case, the mixing angles in the chargino sector read

$$\theta_{U,V} \simeq \arctan \left[ \frac{\pm 2M_W^2 \frac{1-\tan^2 \beta}{1+\tan^2 \beta} - 2\sqrt{(M_W^2 + \mu_{\text{eff}}^2)^2 - \mu_{\text{eff}}^4}}{\sqrt{2} M_W \mu_{\text{eff}} (1 + \tan \beta)} \right], \quad (7)$$

where  $m_W$  is the mass of  $W$  boson. The sign of the first term implies that the enhancement can only be seen when  $a_2$  has a leading  $H_{dI}$  component so that the term in eq. (7) proportional to  $\sin \theta_U \cos \theta_V$  is dominant. Evidently, in such a case the  $a_2 b\bar{b}$  coupling and in turn  $\text{BR}(a_2 \rightarrow b\bar{b})$  will also get enhanced. Consequently, a contribution from  $a_2$  will provide no significant excess in the  $\gamma\gamma$  signal rate, defined in eq. (2).

The above explanation also precludes such a scenario in the MSSM, where the pseudoscalar,  $A$ , is doublet-like. Besides, as noted in [33, 34], in the MSSM in order to obtain a lightest CP-even Higgs boson,  $h$ , with mass around 125 GeV,  $m_A$  is required to be  $\gtrsim 300$  GeV, which is the so-called decoupling regime of the model. On the other hand, while it is also possible to have a  $\sim 125$  GeV  $H$ , the heavier CP-even Higgs boson of the MSSM, this can only be achieved for  $95 \text{ GeV} < m_A < 110 \text{ GeV}$ , in a tiny portion of the ‘non-decoupling regime’. This region is, moreover, disfavored by the constraints from flavor physics [35, 36].

In the fully constrained version of the NMSSM, unification of  $A_\kappa$  and  $A_0$  at the GUT scale introduces tension between the masses of  $h_1$  and  $a_1$ , not allowing both to acquire values  $\lesssim 125$  GeV simultaneously. There, in order to obtain the correct  $h_1$  mass, large negative values of  $A_0$  are necessary so that the mixing term ( $\frac{X_t}{M_{\text{SUSY}}} \simeq \frac{A_t}{M_{\text{SUSY}}}$ ) can be maximized. A light  $a_1$ , on the other hand requires small  $A_\kappa$  at  $M_{\text{SUSY}}$ , which in turn implies small  $A_\kappa$  at the GUT scale, owing to the effects of running. Moreover, small values of  $\mu_{\text{eff}}$ , necessary to obtain light higgsino-like charginos, additionally limit the running of  $A_t$  in the CNMSSM [14]. Therefore, to obtain a SM-like  $\sim 125$  GeV  $h_1$  and a pseudoscalar with a similar mass and a non-negligible  $\gamma\gamma$  rate one has to look beyond the MSSM and the CNMSSM, hence we analyse the CNMSSM-NUHM here.

Through the mechanism explained above, a more precise measurement of the reduced effective coupling,  $C_{a_1}(\gamma\gamma) \equiv \frac{C_{a_1}^{\text{eff}}(\gamma\gamma)}{C_{h_{\text{SM}}}^{\text{eff}}(\gamma\gamma)}$ , can yield an effective limit on the mass of the lighter chargino through<sup>2</sup>

$$C_{a_1}(\gamma\gamma) \simeq \lambda \times \frac{130 \text{ GeV}}{m_{\chi_1^\pm}}, \quad (8)$$

---

<sup>2</sup>Assuming a singlet-like  $a_1$ , which implies  $P_{13} \simeq 1$ , and a higgsino-like  $\chi_1^\pm$  so that  $\sin \theta_{U,V} \simeq 1$ .

for  $m_{a_1} \simeq 125$  GeV. The bound obtained on the mass of  $\chi_1^\pm$  is also an effective upper limit on the mass of the lightest neutralino,  $\chi$  ( $\equiv \chi_1^0$ ).

Having described the mechanism for enhancing the  $\gamma\gamma$  decay rate of  $a_1$ , we now discuss the actual quantity used for comparison with the experimentally observed  $\gamma\gamma$  rate. In terms of the reduced effective couplings,  $C_{a_1}(\gamma\gamma)$  and  $C_{a_1}(d\bar{d})$ , of  $a_1$  to  $\gamma\gamma$  and  $b\bar{b}$ , respectively, the signal rate, given in eq. (2), can be rewritten, specifically for the aforementioned associated production mode with a  $b\bar{b}$  pair in the final state, as

$$R_{\gamma\gamma}^{bb}(a_1) = C_{a_1}^2(d\bar{d}) C_{a_1}^2(\gamma\gamma) \frac{\Gamma_{h_{SM}}^{\text{total}}}{\Gamma_{a_1}^{\text{total}}} \simeq |P'_{11}|^2 \lambda^2 \tan^2 \beta \left( \frac{130 \text{ GeV}}{m_{\chi_1^\pm}} \right)^2 \left( \frac{1}{\Gamma_{a_1}^{\text{total}}/\Gamma_{h_{SM}}^{\text{total}}} \right), \quad (9)$$

where  $|P'_{11}| \simeq \left| \frac{\lambda(A_\lambda^{\text{SUSY}} - 2\kappa s)v}{\mu(A_\lambda^{\text{SUSY}} - \kappa s)\tan\beta} \right|$  and  $\Gamma_{h_{SM}}^{\text{total}}$  denoting the theoretical value of the total width of a SM Higgs boson with the same mass as  $a_1$ . Note that while larger values of  $\tan\beta$  are preferred by  $C_{a_1}^2(d\bar{d})$  in the first equality in the above equation (and also  $C_{h_1}^2(d\bar{d})$  in the corresponding equation for  $R_{\gamma\gamma}^{bb}(h_1)$ ), there is a further dependence on  $\tan\beta$  in  $\Gamma_{h_{SM}}^{\text{total}}/\Gamma_{a_1}^{\text{total}}$  which is not as straightforward.

In the following section we will use eqs. (8) and (9) to obtain an effective upper limit on  $m_{\chi_1^\pm}$  and the mass of  $\chi$ ,  $m_\chi$ , in our model under consideration.

### 3 The CNMSSM-NUHM

In the fully constrained NMSSM universality conditions are imposed on the dimensionful parameters at the GUT scale. This leads to a unified gaugino mass parameter,  $m_{1/2}$ , in the model Lagrangian, a unified scalar soft SUSY-breaking mass parameter, besides  $m_0$  and  $A_0$ , to which  $A_\lambda$  and  $A_\kappa$  are also unified. These three parameters are thus the only free parameters in the CNMSSM besides the dimensionless Higgs coupling  $\lambda$  which is taken as an input parameter at  $M_{\text{SUSY}}$ , given the correct value of the mass of  $Z$  boson,  $m_Z$ .

In the partially unconstrained version of the model, the CNMSSM-NUHM, the soft masses of the Higgs fields,  $m_{H_u}$ ,  $m_{H_d}$  and  $m_S$ , as well as the soft trilinear coupling parameters  $A_\lambda$  and  $A_\kappa$  are taken as free parameters at the GUT scale, instead of assuming their unification with  $m_0$  and  $A_0$ , respectively. Through the minimization conditions of the Higgs potential the three mass parameters  $m_{H_u}$ ,  $m_{H_d}$  and  $m_S$  at the electroweak scale can be traded for the dimensionless singlet triple-coupling  $\kappa$  and the parameters  $\mu_{\text{eff}}$  and  $\tan\beta$ . The model is thus defined in terms of the following eight continuous input parameters:

$$m_0, m_{1/2}, A_0, \tan\beta, \lambda, \kappa, \mu_{\text{eff}}, A_\lambda = A_\kappa.$$

The unification of  $A_\lambda$  and  $A_\kappa$  at the GUT scale assumed here is in general not necessary in the CNMSSM-NUHM. In fact, one can argue that the restriction on  $A_0$  for  $\mu_{\text{eff}} < 0$  and the resultant tension between  $m_{h_1}$  and  $m_{a_1}$  discussed in the previous section can be relaxed by not imposing such a condition. In that case, the affect of large  $A_\lambda$  can be counter-balanced by increasing  $A_\kappa$  independently, thus still yielding physical  $a_1$  solutions. However, this unification condition has minimal impact on the allowed parameter space of the model for our purpose, since, as we shall see later, we can still exploit the interesting phenomenology of the model while keeping the free parameters to a minimum. This is also consistent with the fully constrained version of the model we studied earlier [14], where  $A_\kappa$  and  $A_\lambda$  are set equal to  $A_0$  at the GUT scale even though  $m_S \neq m_0$ .

In the CNMSSM-NUHM, the upper limit on  $m_{\chi_1^\pm}$  and  $m_\chi$ , as discussed in the previous section, can be obtained from Fig. 1, where  $C_{a_1}(\gamma\gamma)$  and  $R_{\gamma\gamma}^{bb}(a_1)$  are shown as functions of  $m_{\chi_1^\pm}$  in (a) and (b), respectively. For all points in the plots we assume  $122 \text{ GeV} < m_{h_1, a_1} < 130 \text{ GeV}$ .



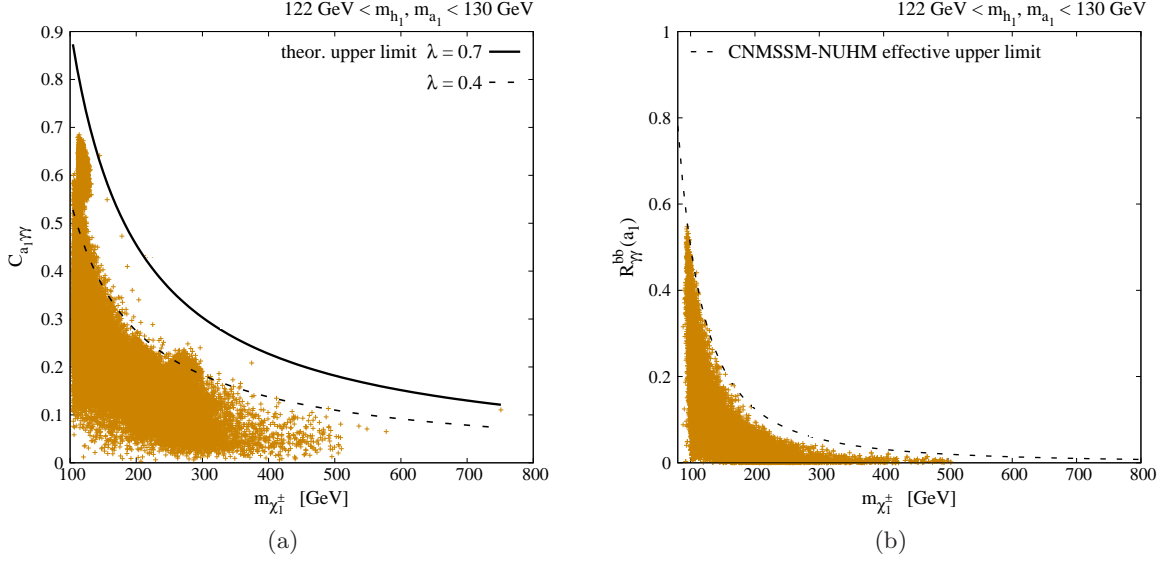


Figure 1: (a) Distribution of points obtained in our scan of the CNMSSM-NUHM parameter space in the  $(m_{\chi_1^\pm}, C_{a_1}(\gamma\gamma))$  plane. The dashed line shows the effective upper limit observed in the scan. The solid line is based on a perturbative upper limit on  $\lambda$  and is shown for comparison. (b) Distribution of points in the  $(m_{\chi_1^\pm}, R_{\gamma\gamma}^{bb}(a_1))$  plane. The dashed line shows the effective upper limit observed in our scan.

## 4 Methodology and results

We perform scans of the parameter space of CNMSSM-NUHM requiring the masses of  $h_1$  and  $a_1$  to be 125.5 GeV, with the theoretical and experimental errors taken in quadrature as 3 GeV around this mean. We impose the latest 95% confidence level (CL) exclusion limit on SUSY provided by the ATLAS collaboration [37].<sup>3</sup> We additionally include Gaussian likelihoods for the most significant  $b$ -physics observables, with their measured mean values and errors taken as:

- $\text{BR}(B_s \rightarrow \mu^+ \mu^-) = (3.2_{-1.2}^{+1.5} \pm 0.32) \times 10^{-9}$ ,
- $\text{BR}(B_u \rightarrow \tau \nu) = (1.66 \pm 0.66 \pm 0.38) \times 10^{-4}$ ,
- $\text{BR}(\overline{B} \rightarrow X_s \gamma) = (3.43 \pm 0.22 \pm 0.21) \times 10^{-4}$  and
- $\Delta M_{B_s} = (17.72 \pm 0.04 \pm 2.4) \text{ ps}^{-1}$ .

For testing the compatibility of the regions of interest against the direct detection cross section,  $\sigma_p^{\text{SI}}$ , we use the XENON100 90% CL exclusion limits [38]. Note that we neglect the  $a_\mu$  constraint here, since it is well known that the regions where correct  $a_\mu$  can be obtained in the parameter spaces of SUSY models with unification of squark and slepton soft masses are strongly disfavored by the direct SUSY searches at the LHC [39, 14, 7].

The numerical analysis was performed using the BayesFITS package which engages several external, publicly available tools: MultiNest [40] for sampling of the CNMSSM-NUHM parameter

<sup>3</sup>These limits were originally published assuming the CMSSM. However, it has been verified in [14, 7] that they have negligible dependence on the Higgs sector parameters and are, therefore, applicable to any R-parity conserving SUSY model with unified  $m_0$  and  $m_{1/2}$ .

space; NMSSMTools v3.2.4 [41] for computing SUSY mass spectrum, Higgs BRs and reduced couplings, as well as  $\Delta M_{B_s}$  for a given NMSSM point; SuperIso v3.3 [42] for calculating  $\text{BR}(\bar{B} \rightarrow X_s \gamma)$ ,  $\text{BR}(B_s \rightarrow \mu^+ \mu^-)$  and  $\text{BR}(B_u \rightarrow \tau \nu)$ . DM observables such as the relic density and  $\sigma_p^{\text{SI}}$  are calculated with MicrOMEGAs v2.4.5 [43].

As noted in the previous section, the scenario under consideration requires low values of  $\mu_{\text{eff}}$  giving a light higgsino-like  $\chi_1^\pm$  and correspondingly a  $\chi$  with significant higgsino component. In fact, the CNMSSM-NUHM parameter space conforming to this scenario can be divided into three main regions depending on the composition of  $\chi$ : i) the Focus Point (FP) region, ii) the higgsino region and iii) the singlino-higgsino region. Below we discuss the results for each of these regions separately. We note here that in all our results we show points with neutralino relic density,  $\Omega_\chi h^2$ , lying in the  $\pm 2\sigma$  range,  $0.087 < \Omega_\chi h^2 < 0.137$ , after taking into account 10% error on the theoretical calculation. Also, we use slightly extended range of the allowed Higgs mass,  $122 \text{ GeV} < m_{h_1, a_1} < 130 \text{ GeV}$ , compared to the mass measurements of the observed boson at the LHC in order to allow larger values of theoretical errors. Finally, for all the points considered,  $h_1$  is always SM-like, with  $R_{\gamma\gamma}^{bb}(h_1) \simeq 1$  and  $R_{ZZ/WW}^{bb}(h_1) \simeq 1$ .

#### 4.1 The focus-point region

A light neutralino with mixed bino-higgsino composition can generate correct DM relic density,  $\Omega_\chi h^2$ , in the so called focus-point (FP) region of minimal SUSY models in general [44]. We observed in our preliminary scans that this region better satisfies the constraints from XENON100 and  $\text{BR}(b \rightarrow s \gamma)$  measurement with  $\mu_{\text{eff}} < 0$ , so we shall pursue this case here. In Fig. 2a we show the region in the  $(m_0, m_{1/2})$  plane generating a light  $a_1$  ( $122 \text{ GeV} \leq m_{a_1} \leq 130 \text{ GeV}$ ) and  $\chi$  with a dominant bino and a small higgsino component. In the figure light blue squares correspond to points with  $1 < R_{\gamma\gamma}^{bb}(h_1 + a_1) \leq 1.15$  and green squares to points with  $1.15 < R_{\gamma\gamma}^{bb}(h_1 + a_1) \leq 1.3$ . We see that while large values of  $m_0$  are favored in order to enhance the mass of  $h_1$ ,  $m_{1/2}$  is typically low, which is necessary for producing a mixed bino-higgsino  $\chi$ . This region, however, lies very close to the current 95% CL exclusion limit from ATLAS (also shown in the plot) and should potentially be tested soon.

In Fig. 2b we show the favored ranges of the  $A_0$  and  $\tan \beta$  parameters.  $\tan \beta$  is almost always  $\gtrsim 5$  to allow enhancement in the  $h_1 b \bar{b}$  coupling in our considered Higgs production mode, as noted earlier. However, we see in the figure that for high positive  $A_0$   $\tan \beta$  is limited to small values,  $\lesssim 15$ . The reason is that large  $\tan \beta$  results in an enhanced Yukawa coupling of  $h_1$  to  $b \bar{b}$  and  $\tau \bar{\tau}$ . Consequently  $A_\lambda$  runs downwards rapidly from its GUT scale value (we shall see below that large positive  $A_0$  coincides with negative  $A_\lambda$ ) to more negative values at  $M_{\text{SUSY}}$ . This in turn causes  $A_\kappa$  to run upwards from its GUT scale value, raising  $m_{a_1}$  beyond its desired value. The effective upper bound on  $\tan \beta$  is relaxed for lower  $|A_0|$ , when the running is slower.

In Fig. 2c we show the distribution of the parameters  $A_0$  and  $A_\kappa = A_\lambda$  at the GUT scale. We notice that  $A_0$  stops at much smaller negative values than it would be expected to take in order to maximize  $m_{h_1}$ . This is due to the same reason as explained in Sec. 2. The main contribution to  $m_{a_1}$  comes from the leading term in eq. (3). Since in this region we assume  $\mu_{\text{eff}} < 0$ ,  $A_0$  is strongly bounded from below in order to minimize the affect of the second term there. Such negative  $A_0$ , by causing positive  $A_\lambda$  to run upwards, also pushes  $A_\kappa$  to somewhat large positive values at the GUT scale resulting in its small positive values at  $M_{\text{SUSY}}$ , since it runs in the opposite direction to  $A_\lambda$ . This is also the reason why no points are visible in the region with negative  $A_\kappa$  and negative  $A_0$ , but one can see some points with positive  $A_\kappa$  and positive  $A_0$ . Finally, for negative  $A_\kappa$  large positive  $A_0$  can be reached, since such values of  $A_0$  drive positive  $A_\lambda$  at the GUT scale downwards, which in turn causes  $A_\kappa$  to run upwards to positive values at  $M_{\text{SUSY}}$ .



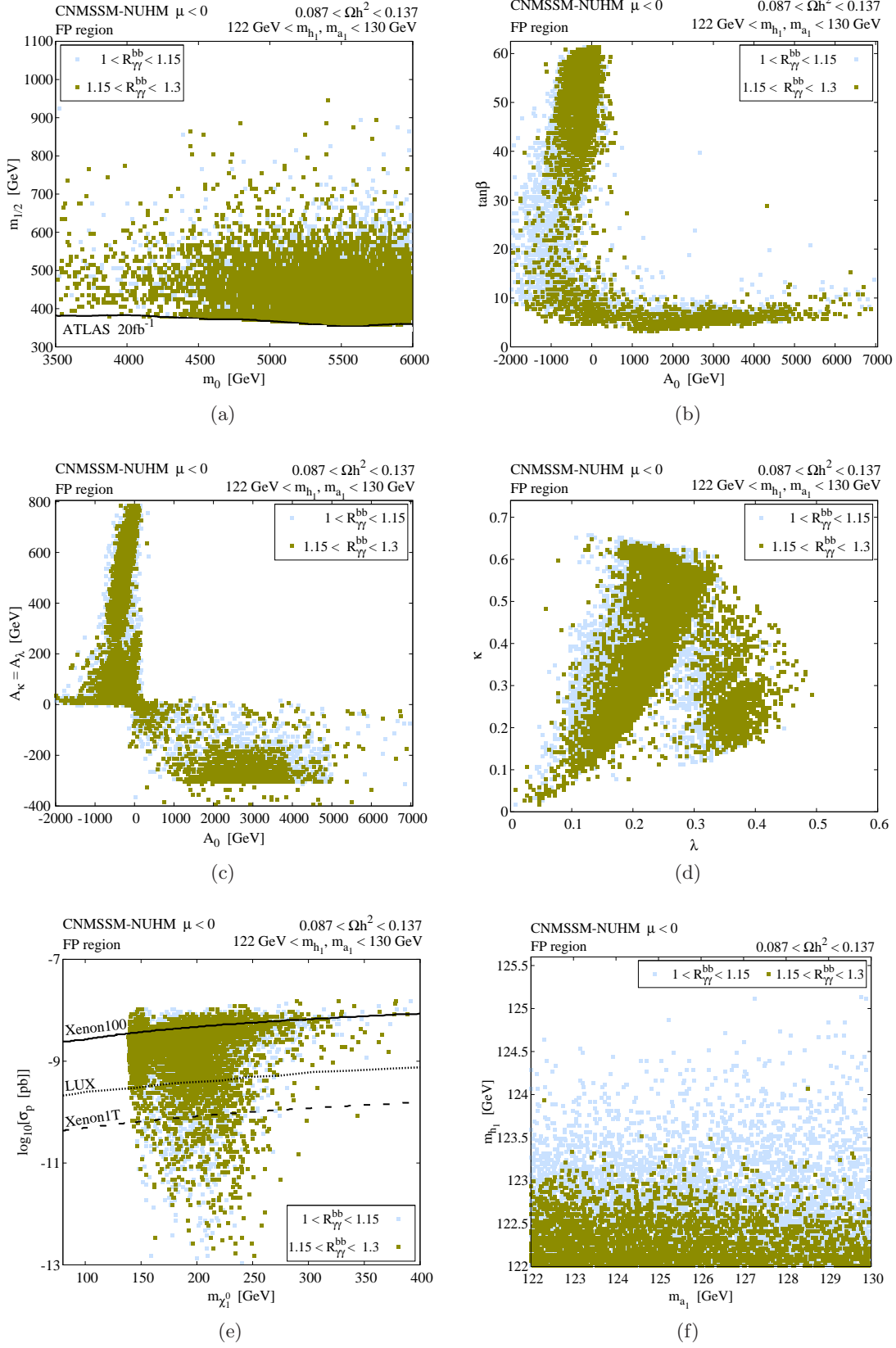


Figure 2: (a)-(d) Ranges of CNMSSM-NUHM parameters corresponding to the FP region. (e)  $\sigma_p^{\text{SI}}$  obtained for this region as a function of  $m_{\chi}$ . (f) Ranges of  $m_{h_1}$  and  $m_{a_1}$  obtained in this region. See text for details.

Fig. 2d shows the ranges of  $\lambda$  and  $\kappa$  corresponding this scenario. While  $\kappa$  is widely distributed, the allowed range of  $\lambda$  is subject to a three-way tension. Large  $\lambda$  is favored in order to obtain an enhancement in the coupling of  $a_1$  to  $\chi_1^\pm$  but the condition to obtain a SM-like  $h_1$ , on the other hand, prefers smaller values. The small-to-intermediate range of  $\lambda$  seen in the figure is then a result of the compromise between these two conditions and, additionally, of the requirement to achieve the desired  $m_{a_1}$  by generating  $s$  ( $= \mu_{\text{eff}}/\lambda$ ) of the correct size.

In Fig. 2e we show how the points in the FP region yielding such a scenario fare against the XENON100 limits. Also shown in the figure are the actual 90% CL exclusion limits from XENON100 as well as the 90% CL limits expected from the LUX [45] and XENON1T [46] experiments. Note that  $m_\chi$  is bounded from below by the ATLAS limit on  $m_{1/2}$  in this region as it is bino-dominated. We see that a majority of the allowed points with an enhanced  $\gamma\gamma$  rate lie below the XENON100 line. Most of this region, however, lies above the LUX limit, while the XENON1T data should be able to test almost all of it. Fig. 2f shows the allowed masses of  $h_1$  and  $a_1$  in this region. We see that  $m_{h_1}$  is always lighter than 124 GeV, which is a consequence of the not very large values of negative  $A_0$  allowed in this region, as discussed above.  $a_1$ , on the other hand, can easily have a mass around 125 GeV.

Overall, we notice only slight enhancement, up to  $\sim 25\%$  in the  $\gamma\gamma$  rate compared to the SM expectation in this region of the CNMSSM-NUHM parameter space. The reason being that  $m_{\chi_1^\pm}$  is not allowed to take small enough value due to the lower bound on the mass of  $\chi$  discussed above ( $m_{\chi_1^\pm} \simeq \mu_{\text{eff}} > m_\chi$ ).  $\text{BR}(B_s \rightarrow \mu^+ \mu^-)$  in this region varies between  $2 \times 10^{-9}$  and  $5.5 \times 10^{-9}$ , which is within  $2\sigma$  of the experimentally measured value  $3.2 \times 10^{-9}$ , taking into account the theoretical error (as in [14]). On the other hand,  $\text{BR}(b \rightarrow s\gamma)$  takes values between  $3.1 \times 10^{-4}$  and  $3.7 \times 10^{-4}$  and hence is always close to the experimental value. This region, owing mainly to the facts that  $m_{h_1}$  finds it difficult to reach the experimentally observed value and that the reduced  $\gamma\gamma$  rate of  $a_1$  barely exceeds 0.25, is the least favored of the three regions explored here.

## 4.2 The higgsino region

A nearly pure higgsino-like neutralino can generate large enough  $\Omega_\chi h^2$  only if  $m_\chi \simeq \mu_{\text{eff}} \sim 1$  TeV [7], but such high values of  $\mu_{\text{eff}}$  will not yield the desired enhancement in the  $a_1 \rightarrow \gamma\gamma$  rate. Therefore, in order to obtain a sizeable enhancement one has to relax the condition on neutralino relic density (thereby allowing low  $\mu_{\text{eff}}$  and, therefore,  $\Omega_\chi h^2$  to be too low). One can assume that a neutralino contributes only partially to the relic abundance of the universe beside some other DM candidate. In that case  $\Omega_\chi h^2 = \xi \Omega_{\text{total}} h^2$ , where  $\xi$  is the fraction of the total relic abundance produced by  $\chi$  and  $\Omega_{\text{total}} h^2 = 0.112$ . Another possibility is that the entire relic abundance is due to an alternative DM candidate particle in the model. Often considered examples of such an additional/alternative DM candidate are gravitino (see, e.g., [47] for recent analyses in the MSSM) and/or axino [48]. The first (second) of these candidates is (not) tightly constrained by Big Bang Nucleosynthesis but both are likely to be allowed in this region due to the low neutralino yield at freeze-out.

In Fig. 3a we show the region in the  $(m_0, m_{1/2})$  plane generating a light  $a_1$  and a higgsino-like  $\chi$ . Light blue squares correspond to points with  $1 < R_{\gamma\gamma}^{bb}(h_1 + a_1) \leq 1.15$ , green squares to points with  $1.15 < R_{\gamma\gamma}^{bb}(h_1 + a_1) \leq 1.3$ , red squares to points with  $1.3 < R_{\gamma\gamma}^{bb}(h_1 + a_1) \leq 1.45$  and green squares to points with  $1.45 < R_{\gamma\gamma}^{bb}(h_1 + a_1)$ . Large values of  $m_0$  are preferred in order to enhance  $m_{h_1}$  through radiative corrections from the SUSY sector.  $m_{1/2}$  also takes large values in order to minimize the bino component of  $\chi$  with large  $\mu_{\text{eff}}-m_{1/2}$  splitting.

In Fig. 3b the favored ranges of  $\tan\beta$  and  $A_0$  parameters are shown. We see that the enhancement in  $R_{\gamma\gamma}^{bb}(h_1 + a_1)$  decreases as  $\tan\beta$  increases. The reason for this is as follows. The

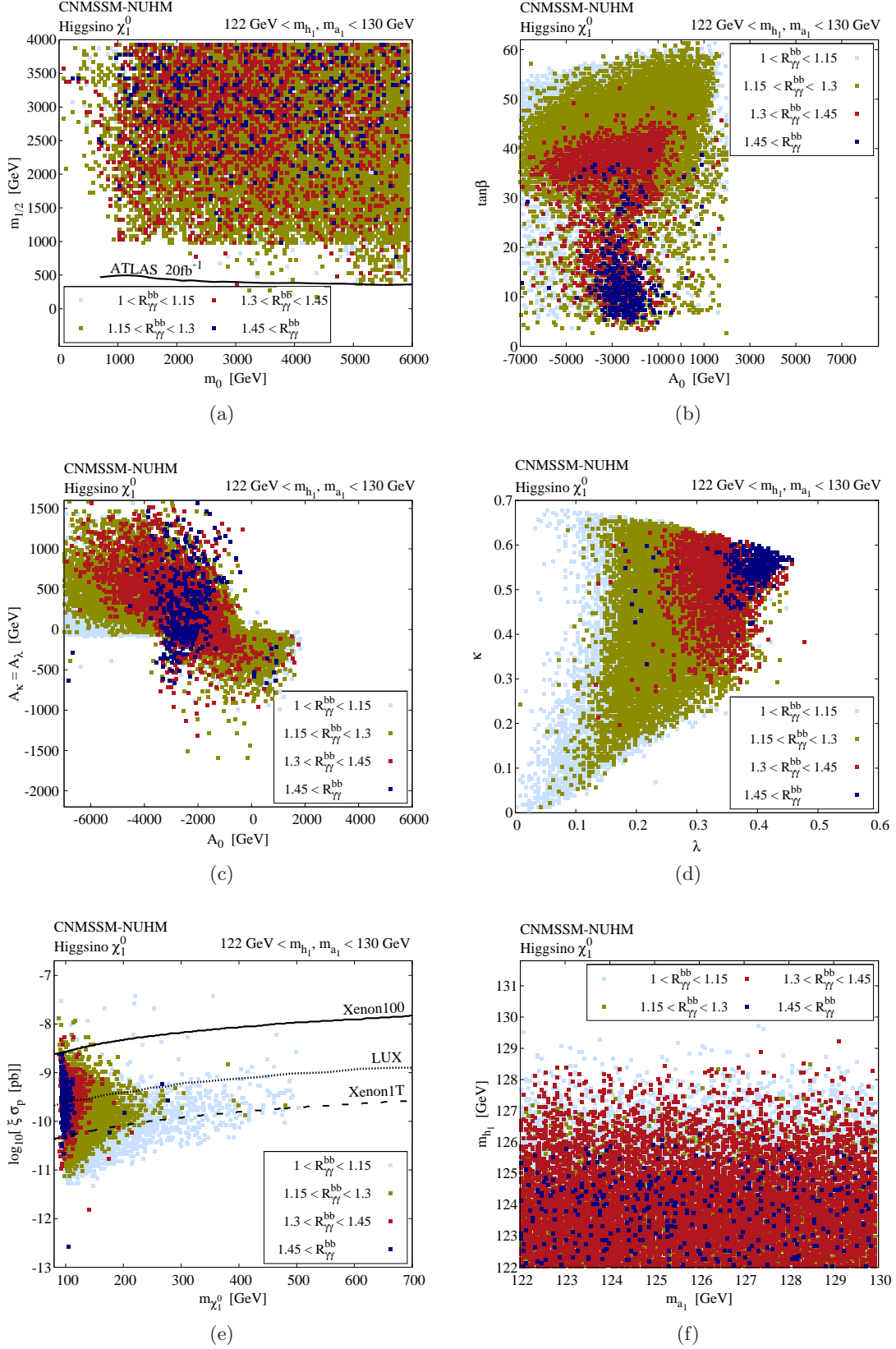


Figure 3: (a)-(d) Ranges of CNMSSM-NUHM parameters corresponding to the higgsino region. (e)  $\xi \sigma_p^{SI}$  obtained for this region as a function of  $m_\chi$ , where  $\xi = \Omega_\chi h^2 / \Omega_{\text{total}} h^2$ . (f) Ranges of  $m_{h_1}$  and  $m_{a_1}$  obtained in this region. See text for details.

enhancement in  $R_{\gamma\gamma}^{bb}(a_1)$  grows with  $\lambda$ , according to eq. (9). However, large values of  $\lambda$  can only give correct  $m_{h_1}$  for not too large values of  $\tan\beta$ . This is because larger values of  $\tan\beta$  result in an enhanced Yukawa coupling of  $h_1$  to  $b\bar{b}$  and  $\tau\bar{\tau}$ . This will make  $A_\lambda$  run upwards faster from its GUT scale value, which in turn causes  $A_\kappa$  to run downwards to larger negative values. That will result in a decrease in  $m_{h_1}$ , since it has a significant singlet component, while  $m_{a_1}$  increases. We point out here that an opposite affect of  $\tan\beta$  was noted in the FP region due to the fact that there  $A_0$  was positive which made  $A_\lambda$  and  $A_\kappa$  run in the opposite directions to those here.

Since for this region  $\mu_{\text{eff}} > 0$ , the effective constraint on  $A_0$  from  $A_\lambda$  applicable in the FP region is relaxed here and larger values of negative  $A_0$  are allowed so that  $m_{h_1}$  can be maximized. The interdependence of  $A_0$  and  $A_\lambda = A_\kappa$  is further illustrated by Fig. 3c.  $A_\kappa$  can take much bigger positive values at the GUT scale, even though it ought to be negative at  $M_{\text{SUSY}}$ . Moreover, a considerable number of points is visible for negative  $A_\kappa$  and negative  $A_0$  up to  $\sim -2$  TeV in contrast with the FP region. The reason is, again, the fact that here negative  $A_0$  makes  $A_\lambda$  run upwards between the GUT scale and  $M_{\text{SUSY}}$  and since the latter is negative it also drives  $A_\kappa$  upwards to smaller negative values. Naturally then, negative  $A_0$  should not be too large or  $A_\kappa$  at  $M_{\text{SUSY}}$  will be driven positive. For positive  $A_\kappa$  only large negative  $A_0$  values are allowed because  $A_\lambda$  is also positive now and so the running of  $A_\kappa$  switches to downward direction. Positive  $A_0$  solutions are also possible, as in the FP region, as long as they don't yield positive  $A_\kappa$  at  $M_{\text{SUSY}}$ .

In Fig. 3d the ranges of the parameters  $\lambda$  and  $\kappa$  favored by our proposed scenario are shown for this region. While  $\kappa$  is as widely distributed as in the FP region, comparatively slightly larger values of  $\lambda$  are possible in this region since  $s$  is more free to vary owing to the less constrained  $A_\kappa$ . In Fig. 3e we show the distribution of the points in the  $(m_\chi, \xi\sigma_p^{\text{SI}})$  plane for this region.<sup>4</sup> Almost all the points obtained in this region lie below the XENON100 line and a portion of these points even lies below the projected XENON1T line. Since  $\chi$  is almost purely higgsino here, the smaller its mass the bigger the enhancement in  $R_{\gamma\gamma}^{bb}(a_1)$  is generated. Moreover, this region corresponds to large values of  $m_0$  and  $m_{1/2}$  so that the squarks and gluinos are always much heavier than the current LHC reach. Nevertheless, as discussed earlier, a more precise measurement of  $R_{\gamma\gamma}^{bb}$  could still introduce limits on  $m_\chi$  and  $m_{\chi_1^\pm}$ . Such derived upper limits are, therefore, especially interesting from the experimental point of view.

Finally, as a result of larger allowed values of negative  $A_0$ ,  $h_1$  as heavy as 129 GeV can be obtained in this region, as can be seen in Fig. 3f.  $a_1$  mass is evenly distributed in the defined range, almost always showing a large enhancement in the  $\gamma\gamma$  rate. Finally, compared to the FP region, a majority of points in this region show a big enhancement, up to  $\sim 50\%$  above the SM expectation, in the  $\gamma\gamma$  rate in this region. We also note here that both  $\text{BR}(B_s \rightarrow \mu^+\mu^-)$  and  $\text{BR}(b \rightarrow s\gamma)$  always lie around their respective SM values.

### 4.3 The singlino-higgsino region

This region is defined by  $\chi$  being an admixture of a large higgsino component and a smaller but important singlino component. Owing to the significant singlino component (20%–30%) the neutralino will interact very weakly with matter and will thus result in large relic abundance unless it has a small mass and consequently large annihilation cross-section. In Fig. 4a we see the distribution of this region in the  $(m_0, m_{1/2})$  plane. The color assignment of the points is the same as in the higgsino region. Large values of  $m_0$  and intermediate values of  $m_{1/2}$  are favored, again, for allowing a higgsino-like neutralino with smaller positive  $\mu_{\text{eff}}$ . In Fig. 4b we see that once again

---

<sup>4</sup>The figure assumes that  $\chi$  is only responsible for a small portion of the observed relic abundance. For the points obtained in the scan  $\xi \leq 0.05$ .

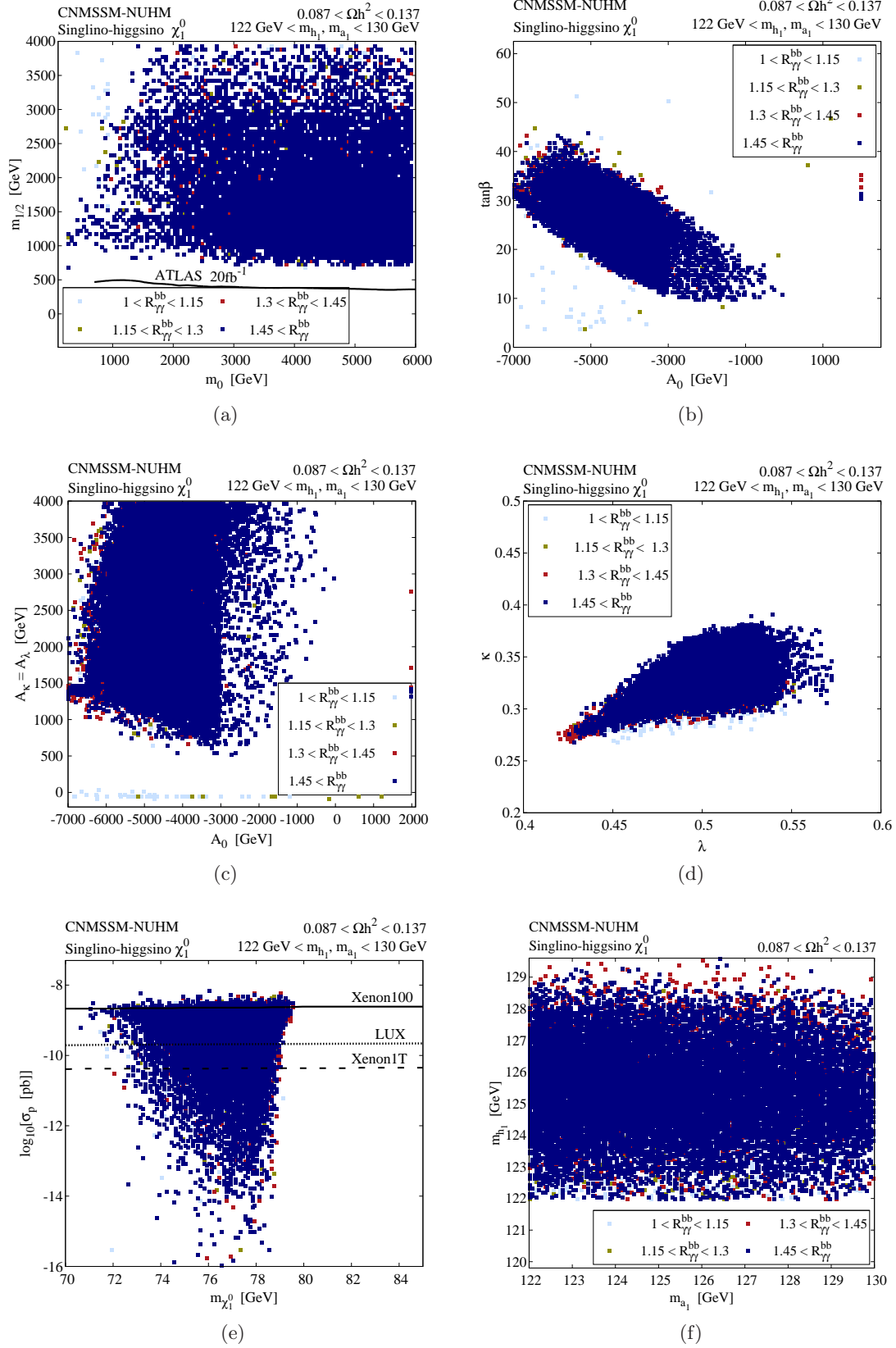


Figure 4: (a)-(d) Ranges of CNMSSM-NUHM parameters corresponding to the singlino-higgsino region. (e)  $\sigma_p^{\text{SI}}$  obtained for this region as a function of  $m_{\chi}$ . (f) Ranges of  $m_{h_1}$  and  $m_{a_1}$  obtained in this region. See text for details.

$\tan\beta$  spans a fairly wide range but its small to intermediate values are favored by  $R_{\gamma\gamma}^{bb}(a_1)$ , for the same reasons as in the higgsino region.  $A_0$  almost always takes large negative values, in order to maximize  $m_{h_1}$ . In contrast with the higgsino region, there are hardly any points corresponding to positive  $A_0$ .

In Fig. 4c we show the distribution of points in the  $(A_0, A_\kappa)$  plane and in Fig. 4d in the  $(\lambda, \kappa)$  plane. The observed range of  $\kappa$  is smaller compared to the previous regions while that of  $\lambda$  is larger. This is in fact the main feature distinguishing this region from the higgsino region in terms of the parameter space of the model. Larger values of  $\lambda$  and small values of  $\kappa$  are required to maximize the singlino component of  $\chi$ , as the  $5 \times 5$  term in the neutralino mass matrix is equal to  $2\kappa s$  ( $\equiv 2\kappa\mu_{\text{eff}}/\lambda$ ). Hence the smallness in  $\kappa$  has to be compensated by slightly larger values of  $A_\kappa$  compared to the previous two regions, as noted in Fig. 4c, for obtaining the correct  $m_{a_1}$ . Finally, like the other two regions, the largest enhancement in  $R_{\gamma\gamma}^{bb}(a_1)$  is obtained for largest possible values of  $\lambda$ .

In Fig. 4e we show the  $(m_\chi, \sigma_p^{\text{SI}})$  plane for this region. A large number of points satisfying the XENON100 limit lies below the projected 90% CL XENON1T limit. Note also that since much smaller  $m_\chi$  and consequently  $m_{\chi_1^\pm}$  is favored by this region compared to the other two, almost all the points below the XENON100 line have a highly enhanced  $R_{\gamma\gamma}^{bb}(a_1)$ , since  $\chi_1^\pm$  also appears in the denominator of eq. (9). This is also the reason why such points are achievable even with relatively small values of  $\tan\beta$ , as seen in Fig. 4b earlier. This region is thus the one yielding maximum enhancement, up to  $\sim 60\%$  or so, in  $R_{\gamma\gamma}^{bb}(h_1 + a_1)$  out of the three regions discussed here and is, therefore, the most favorable for all.

In Fig. 4f we show the distribution of  $m_{h_1}$  versus that of  $m_{a_1}$ . We note that this region yields mostly larger  $m_{h_1}$  compared to the previous two regions, which is due to the combined effects of large negative  $A_0$  as well as larger allowed values of  $\lambda$ . Another distinguishing feature of this region is that  $h_2$  can also be almost mass degenerate with  $h_1$  and  $a_1$ , implying in that case a ‘triple degeneracy’ among the Higgses. Again, while mass degenerate  $h_1$  and  $h_2$  can explain the enhanced  $\gamma\gamma$  rate in the  $ggh$  production mode in the ATLAS data, in order to test the additional degeneracy with  $a_1$  one will have to explore the associated production mode of Higgs with  $b\bar{b}$ . In the  $b\bar{b}h$  production mode, such  $h_2$  can further contribute  $\sim 20\%$  of the measured  $\gamma\gamma$  rate. Finally,  $\text{BR}(B_s \rightarrow \mu^+\mu^-)$  in this region varies between  $3 \times 10^{-9}$  and  $3.8 \times 10^{-9}$  while  $\text{BR}(b \rightarrow s\gamma)$  lies in the  $2.8 \times 10^{-4}$  to  $3.3 \times 10^{-4}$  range.

To conclude, in Fig. 5a we show the range of  $m_\chi$  across all the regions for which an enhancement in  $R_{\gamma\gamma}^{bb}(h_1 + a_1)$  was obtained in our CNMSSM-NUHM scan, and its compatibility with the current and expected limits on  $\sigma_p^{\text{SI}}$ . These regions are identified separately in Fig. 5b, again, in the  $(m_\chi, \xi\sigma_p^{\text{SI}})$  plane, where the orange squares denote the FP region, dark green squares the higgsino region and brown squares the singlino-higgsino region.

## 5 Summary

We have proposed a scenario in the NMSSM in which the lightest pseudoscalar of the model,  $a_1$ , as well a SM-like scalar Higgs boson,  $h_1$ , both have masses around  $\sim 125$  GeV. The pseudoscalar could be distinguishable from the scalar at the LHC in the associated production mode with a  $b\bar{b}$  pair in the final state. This is because it will contribute significantly to the observed signal rate in the  $\gamma\gamma$  channel but, since a pseudoscalar doesn’t couple to  $W$  and  $Z$  bosons, the measured rate in the  $WW/ZZ$  channels will be due only to the scalar and therefore SM-like. The observable enhancement in the  $\gamma\gamma$  rate is made possible by a light chargino entering in the one-loop effective



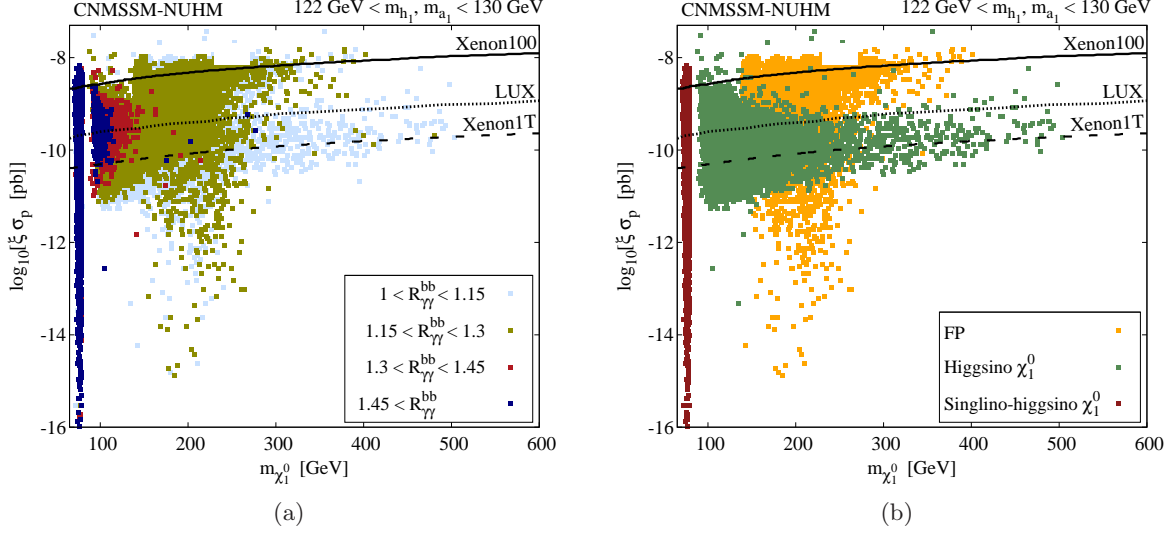


Figure 5: (a) The range of  $\sigma_p^{SI}$  for giving an enhancement in  $R_{\gamma\gamma}^{bb}(h_1 + a_1)$  versus the neutralino mass  $m_{\chi_1^0}$ . Also shown are the 90% CL exclusion limits from XENON100 as well as the 90% CL limits expected from the LUX and XENON1T experiments.  $\xi = \Omega_{\chi} h^2 / \Omega_{\text{total}} h^2$  when  $\chi$  is almost purely higgsino but 1 otherwise. (b) The  $(m_{\chi_1^0}, \sigma_p^{SI})$  plane showing the three CNMSSM-NUHM regions where  $R_{\gamma\gamma}^{bb}(h_1 + a_1)$  is enhanced. Green squares denote the FP region, red squares the higgsino region and blue squares the singlino-higgsino region.  $\xi = \Omega_{\chi} h^2 / \Omega_{\text{total}} h^2$  in the higgsino region, but 1 in the FP and singlino-higgsino regions.

coupling of  $a_1$  to two photons. We have discussed the conditions necessary to obtain  $a_1$  with the correct mass as well as an enhanced  $\gamma\gamma$  rate. We have argued that due to very specific requirements on the composition of  $a_1$ , which should be singlet-like, and of the light chargino, which should be almost purely higgsino-like, such a scenario cannot be realized in the MSSM and is extremely unlikely in the fully constrained NMSSM.

We have, therefore, analyzed the CNMSSM with the universality conditions lifted in the Higgs sector to study our proposed scenario. We have scanned the parameter space of this model in order to look for regions that can allow both  $\chi_1^{\pm}$  and  $a_1$  with the desired masses and compositions. We have found that these regions can be divided into three broad cases, based on the composition of the neutralino which, owing to the condition on  $\chi_1^{\pm}$ , should also have a large higgsino component. These regions include the FP region, where  $\chi$  is a bino-higgsino mixture, the higgsino region, where it is almost purely higgsino, and the singlino region, where it is higgsino-dominated but with an admixture of the singlino. The region least favored by enhancement in the  $\gamma\gamma$  rate of  $a_1$  is the FP region, where it only reaches up to  $\sim 25\%$ , while the most favored one is the singlino region, where the enhancement can be as high as  $\sim 60\%$ .

We noted, however, that such  $a_1$  is likely to remain invisible at the LHC in the gluon-fusion production channel. The reason is that while the effective coupling of  $a_1$  to the  $\gamma\gamma$  pair gets enhanced, the effective coupling to two gluons is still highly suppressed compared to  $h_1$ . We emphasize that a more focussed analysis of the associated Higgs production mode with  $b\bar{b}$  pair, which is the least favorable production mode for a SM-like Higgs, is essential. By revealing such a pseudoscalar, this production mode could provide a clear signature of our proposed model scenario, in particular, and of beyond the SM physics, in general.

## ACKNOWLEDGMENTS

The authors would like to thank Y.-L. Sming Tsai for valuable discussions and inputs. This work has been funded in part by the Welcome Programme of the Foundation for Polish Science. L.R. is also supported in part by the Polish National Science Centre grant N N202 167440, an STFC consortium grant of Lancaster, Manchester and Sheffield Universities and by the EC 6th Framework Programme MRTN-CT-2006-035505. The use of the CIS computer cluster at NCBJ is gratefully acknowledged.

## References

- [1] **CMS Collaboration** Collaboration, S. Chatrchyan *et al.*, “Observation of a new boson at a mass of 125 GeV with the CMS experiment at the LHC,” [arXiv:1207.7235 \[hep-ex\]](#).
- [2] **ATLAS Collaboration** Collaboration, G. Aad *et al.*, “Observation of a new particle in the search for the Standard Model Higgs boson with the ATLAS detector at the LHC,” [arXiv:1207.7214 \[hep-ex\]](#).
- [3] [twiki.cern.ch/twiki/bin/view/CMSPublic/PhysicsResultsHIG](http://twiki.cern.ch/twiki/bin/view/CMSPublic/PhysicsResultsHIG)
- [4] [twiki.cern.ch/twiki/bin/view/AtlasPublic/HiggsPublicResults](http://twiki.cern.ch/twiki/bin/view/AtlasPublic/HiggsPublicResults)
- [5] D. J. Chung, A. J. Long, and L.-T. Wang, “The 125 GeV Higgs and Electroweak Phase Transition Model Classes,” *Phys.Rev.* **D87** (2013) 023509, [arXiv:1209.1819 \[hep-ph\]](#). ; H. Baer, V. Barger, P. Huang, D. Mickelson, A. Mustafayev, *et al.*, “Post-LHC7 fine-tuning in the mSUGRA/CMSSM model with a 125 GeV Higgs boson,” [arXiv:1210.3019 \[hep-ph\]](#). ; Z. Heng, “A 125 GeV Higgs and its di-photon signal in different SUSY models: a mini review,” [arXiv:1210.3751 \[hep-ph\]](#). ; D. Berenstein, T. Liu, and E. Perkins, “Multiple b-jets reveal natural SUSY and the 125 GeV Higgs,” [arXiv:1211.4288 \[hep-ph\]](#). ; K. Cheung, C.-T. Lu, and T.-C. Yuan, “Diphoton Rate of the Standard-Model-Like Higgs Boson in the Extra U(1) Extended MSSM,” *Phys.Rev.* **D87** (2013) 075001, [arXiv:1212.1288 \[hep-ph\]](#). ; J. Cao, L. Wu, P. Wu, and J. M. Yang, “The Z+photon and diphoton decays of the Higgs boson as a joint probe of low energy SUSY models at LHC,” [arXiv:1301.4641 \[hep-ph\]](#).
- [6] A. Fowlie, M. Kazana, K. Kowalska, S. Munir, L. Roszkowski, *et al.*, “The CMSSM Favoring New Territories: The Impact of New LHC Limits and a 125 GeV Higgs,” *Phys.Rev.* **D86** (2012) 075010, [arXiv:1206.0264 \[hep-ph\]](#).
- [7] K. Kowalska, L. Roszkowski, and E. M. Sessolo, “Two ultimate tests of constrained supersymmetry,” [arXiv:1302.5956 \[hep-ph\]](#).
- [8] S. King, M. Muhlleitner, and R. Nevzorov, “NMSSM Higgs Benchmarks Near 125 GeV,” *Nucl.Phys.* **B860** (2012) 207–244, [arXiv:1201.2671 \[hep-ph\]](#). ; J. Cao *et al.*, “A SM-like Higgs near 125 GeV in low energy SUSY: a comparative study for MSSM and NMSSM,” *JHEP* **1203** (2012) 086, [arXiv:1202.5821 \[hep-ph\]](#). ; D. A. Vasquez *et al.*, “The 125 GeV Higgs in the NMSSM in light of LHC results and astrophysics constraints,” [arXiv:1203.3446 \[hep-ph\]](#). ; J. Rathsmann and T. Rossler, “Closing the Window on Light Charged Higgs Bosons in the NMSSM,” [arXiv:1206.1470 \[hep-ph\]](#). ; D. Das, U. Ellwanger, and P. Mitropoulos, “A 130 GeV photon line from dark matter annihilation in the NMSSM,” *JCAP* **1208** (2012) 003, [arXiv:1206.2639 \[hep-ph\]](#). ; M. Carena, S. Gori, I. Low,

- N. Shah, and C. Wagner, “Vacuum Stability and Higgs Diphoton Decays in the MSSM,” *JHEP* **1302** (2013) 114, [arXiv:1211.6136 \[hep-ph\]](#). ; P. Bechtle, S. Heinemeyer, O. Stal, T. Stefaniak, G. Weiglein, *et al.*, “MSSM Interpretations of the LHC Discovery: Light or Heavy Higgs?,” [arXiv:1211.1955 \[hep-ph\]](#).
- [9] J. F. Gunion, Y. Jiang, and S. Kraml, “Could two NMSSM Higgs bosons be present near 125 GeV?,” [arXiv:1207.1545 \[hep-ph\]](#).
- [10] J. F. Gunion, Y. Jiang, and S. Kraml, “Diagnosing Degenerate Higgs Bosons at 125 GeV,” [arXiv:1208.1817 \[hep-ph\]](#).
- [11] R. Benbrik, M. G. Bock, S. Heinemeyer, O. Stal, G. Weiglein, *et al.*, “Confronting the MSSM and the NMSSM with the Discovery of a Signal in the two Photon Channel at the LHC,” [arXiv:1207.1096 \[hep-ph\]](#). ; K. J. Bae, K. Choi, E. J. Chun, S. H. Im, C. B. Park, *et al.*, “Peccei-Quinn NMSSM in the light of 125 GeV Higgs,” [arXiv:1208.2555 \[hep-ph\]](#). ; T. Cheng, J. Li, T. Li, X. Wan, Y. k. Wang, *et al.*, “Toward the Natural and Realistic NMSSM with and without  $R$ -Parity,” [arXiv:1207.6392 \[hep-ph\]](#). ; Z. Kang, T. Li, J. Li, and Y. Liu, “A Radiatively Light Stop Saves the Best Global Fit for Higgs Boson Mass and Decays,” [arXiv:1208.2673 \[hep-ph\]](#). ; M. Perelstein and B. Shakya, “XENON100 Implications for Naturalness in the MSSM, NMSSM and  $\lambda$ -SUSY,” [arXiv:1208.0833 \[hep-ph\]](#). ; K. Schmidt-Hoberg and F. Staub, “Enhanced  $h \rightarrow \gamma\gamma$  rate in MSSM singlet extensions,” *JHEP* **1210** (2012) 195, [arXiv:1208.1683 \[hep-ph\]](#). ; G. Belanger, U. Ellwanger, J. Gunion, Y. Jiang, and S. Kraml, “Two Higgs Bosons at the Tevatron and the LHC?,” [arXiv:1208.4952 \[hep-ph\]](#).
- [12] J. Cao, Z. Heng, J. M. Yang, and J. Zhu, “Status of low energy SUSY models confronted with the LHC 125 GeV Higgs data,” [arXiv:1207.3698 \[hep-ph\]](#).
- [13] G. Chalons and F. Domingo, “Analysis of the Higgs potentials for two doublets and a singlet,” [arXiv:1209.6235 \[hep-ph\]](#). ; I. Gogoladze, B. He, and Q. Shafi, “Inverse Seesaw in NMSSM and 126 GeV Higgs Boson,” [arXiv:1209.5984 \[hep-ph\]](#). ; G. Belanger, U. Ellwanger, J. F. Gunion, Y. Jiang, S. Kraml, *et al.*, “Higgs Bosons at 98 and 125 GeV at LEP and the LHC,” [arXiv:1210.1976 \[hep-ph\]](#). ; H. Dreiner, F. Staub, and A. Vicente, “General NMSSM signatures at the LHC,” *Phys.Rev.* **D87** (2013) 035009, [arXiv:1211.6987 \[hep-ph\]](#). ; T. Gherghetta, B. von Harling, A. D. Medina, and M. A. Schmidt, “The Scale-Invariant NMSSM and the 126 GeV Higgs Boson,” *JHEP* **1302** (2013) 032, [arXiv:1212.5243 \[hep-ph\]](#). ; D. E. Lopez-Fogliani, “Light Higgs and neutralino dark matter in the NMSSM,” *J.Phys.Conf.Ser.* **384** (2012) 012014. ; J. Cao, Z. Heng, L. Shang, P. Wan, and J. M. Yang, “Pair Production of a 125 GeV Higgs Boson in MSSM and NMSSM at the LHC,” [arXiv:1301.6437 \[hep-ph\]](#). ; D. Das, U. Ellwanger, and A. M. Teixeira, “LHC constraints on  $M_{1/2}$  and  $m_0$  in the semi-constrained NMSSM,” [arXiv:1301.7584 \[hep-ph\]](#). ; D. G. Cerdeno, P. Ghosh, and C. B. Park, “Probing the two light Higgs scenario in the NMSSM with a low-mass pseudoscalar,” [arXiv:1301.1325 \[hep-ph\]](#). ; N. D. Christensen, T. Han, Z. Liu, and S. Su, “Low-Mass Higgs Bosons in the NMSSM and Their LHC Implications,” [arXiv:1303.2113 \[hep-ph\]](#). ; W. Wang, J. M. Yang, and L. L. You, “Higgs boson mass in NMSSM with right-handed neutrino,” [arXiv:1303.6465 \[hep-ph\]](#). ; R. Barbieri, D. Buttazzo, K. Kannike, F. Sala, and A. Tesi, “Exploring the Higgs sector of a most natural NMSSM,” [arXiv:1304.3670 \[hep-ph\]](#).

- [14] K. Kowalska, S. Munir, L. Roszkowski, E. M. Sessolo, S. Trojanowski, *et al.*, “The Constrained NMSSM with a 125 GeV Higgs boson – A global analysis,” [arXiv:1211.1693 \[hep-ph\]](#).
- [15] L. Basso and F. Staub, “Enhancing  $h \rightarrow \gamma\gamma$  with staus in SUSY models with extended gauge sector,” *Phys.Rev.* **D87** (2013) 015011, [arXiv:1210.7946 \[hep-ph\]](#). ; K. Schmidt-Hoberg, F. Staub, and M. W. Winkler, “Enhanced diphoton rates at Fermi and the LHC,” *JHEP* **1301** (2013) 124, [arXiv:1211.2835 \[hep-ph\]](#). ; K. Benakli, M. D. Goodsell, and F. Staub, “Dirac Gauginos and the 125 GeV Higgs,” [arXiv:1211.0552 \[hep-ph\]](#). ; P. Athron, S. King, D. Miller, S. Moretti, and R. Nevzorov, “Constrained Exceptional Supersymmetric Standard Model with a Higgs Near 125 GeV,” *Phys.Rev.* **D86** (2012) 095003, [arXiv:1206.5028 \[hep-ph\]](#).
- [16] G. L. Kane, C. F. Kolda, L. Roszkowski, and J. D. Wells, “Study of constrained minimal supersymmetry,” *Phys. Rev.* **D49** (1994) 6173–6210, [arXiv:hep-ph/9312272 \[hep-ph\]](#).
- [17] M. Drees, “Supersymmetric Models with Extended Higgs Sector,” *Int.J.Mod.Phys.* **A4** (1989) 3635.
- [18] J. Ellis, J. F. Gunion, H. E. Haber, L. Roszkowski, and F. Zwirner, “Higgs bosons in a nonminimal supersymmetric model,” *Phys. Rev. D* **39** (Feb, 1989) 844–869. <http://link.aps.org/doi/10.1103/PhysRevD.39.844>
- [19] U. Ellwanger, C. Hugonie, and A. M. Teixeira, “The Next-to-Minimal Supersymmetric Standard Model,” *Phys.Rept.* **496** (2010) 1–77, [arXiv:0910.1785 \[hep-ph\]](#).
- [20] M. Maniatis, “The Next-to-Minimal Supersymmetric extension of the Standard Model reviewed,” *Int.J.Mod.Phys.* **A25** (2010) 3505–3602, [arXiv:0906.0777 \[hep-ph\]](#).
- [21] U. Ellwanger, “A Higgs boson near 125 GeV with enhanced di-photon signal in the NMSSM,” *JHEP* **1203** (2012) 044, [arXiv:1112.3548 \[hep-ph\]](#).
- [22] A. Djouadi, U. Ellwanger, and A. Teixeira, “The Constrained next-to-minimal supersymmetric standard model,” *Phys.Rev.Lett.* **101** (2008) 101802, [arXiv:0803.0253 \[hep-ph\]](#)
- [23] A. Djouadi, U. Ellwanger, and A. Teixeira, “Phenomenology of the constrained NMSSM,” *JHEP* **0904** (2009) 031, [arXiv:0811.2699 \[hep-ph\]](#).
- [24] J. F. Gunion, Y. Jiang, and S. Kraml, “The Constrained NMSSM and Higgs near 125 GeV,” *Phys.Lett.* **B710** (2012) 454–459, [arXiv:1201.0982 \[hep-ph\]](#).
- [25] U. Ellwanger and C. Hugonie, “Higgs bosons near 125 GeV in the NMSSM with constraints at the GUT scale,” [arXiv:1203.5048 \[hep-ph\]](#).
- [26] M. Badziak, M. Olechowski, and S. Pokorski, “New Regions in the NMSSM with a 125 GeV Higgs,” [arXiv:1304.5437 \[hep-ph\]](#).
- [27] **CMS Collaboration** Collaboration, S. Chatrchyan *et al.*, “On the mass and spin-parity of the Higgs boson candidate via its decays to Z boson pairs,” *Phys. Rev. Lett.* **110** (2013) 081803, [arXiv:1212.6639 \[hep-ex\]](#).
- [28] A. Djouadi and G. Moreau, “The couplings of the Higgs boson and its CP properties from fits of the signal strengths and their ratios at the 7+8 TeV LHC,” [arXiv:1303.6591 \[hep-ph\]](#).

- [29] M. Spira, “QCD effects in Higgs physics,” *Fortsch.Phys.* **46** (1998) 203–284, [arXiv:hep-ph/9705337 \[hep-ph\]](#).
- [30] A. Djouadi, “The Anatomy of electro-weak symmetry breaking. II. The Higgs bosons in the minimal supersymmetric model,” *Phys.Rept.* **459** (2008) 1–241, [arXiv:hep-ph/0503173 \[hep-ph\]](#).
- [31] **Particle Data Group** Collaboration, J. Beringer *et al.*, “Review of Particle Physics (RPP),” *Phys.Rev.* **D86** (2012) 010001.
- [32] A. Djouadi, “The Anatomy of electro-weak symmetry breaking. I: The Higgs boson in the standard model,” *Phys.Rept.* **457** (2008) 1–216, [arXiv:hep-ph/0503172 \[hep-ph\]](#).
- [33] N. D. Christensen, T. Han, and S. Su, “MSSM Higgs Bosons at The LHC,” *Phys.Rev.* **D85** (2012) 115018, [arXiv:1203.3207 \[hep-ph\]](#).
- [34] M. Carena, S. Heinemeyer, O. Stl, C. Wagner, and G. Weiglein, “MSSM Higgs Boson Searches at the LHC: Benchmark Scenarios after the Discovery of a Higgs-like Particle,” [arXiv:1302.7033 \[hep-ph\]](#).
- [35] S. Scopel, N. Fornengo, and A. Bottino, “Embedding the 125 GeV Higgs boson measured at the LHC in an effective MSSM: possible implications for neutralino dark matter,” [arXiv:1304.5353 \[hep-ph\]](#).
- [36] C. Boehm, P. S. B. Dev, A. Mazumdar, and E. Pukartas, “Naturalness of Light Neutralino Dark Matter in pMSSM after LHC, XENON100 and Planck Data,” [arXiv:1303.5386 \[hep-ph\]](#).
- [37] “Search for strongly produced superpartners in final states with two same sign leptons with the atlas detector using 21 fb-1 of proton-proton collisions at sqrt(s)=8 tev,” Tech. Rep. ATLAS-CONF-2013-007, CERN, Geneva, Mar, 2013
- [38] **XENON100 Collaboration** Collaboration, E. Aprile *et al.*, “Dark Matter Results from 225 Live Days of XENON100 Data,” [arXiv:1207.5988 \[astro-ph.CO\]](#).
- [39] L. Roszkowski, E. M. Sessolo, and Y.-L. S. Tsai, “Bayesian Implications of Current LHC Supersymmetry and Dark Matter Detection Searches for the Constrained MSSM,” *Phys.Rev.* **D86** (2012) 095005, [arXiv:1202.1503 \[hep-ph\]](#).
- [40] F. Feroz, M. Hobson, and M. Bridges, “MultiNest: an efficient and robust Bayesian inference tool for cosmology and particle physics,” *Mon.Not.Roy.Astron.Soc.* **398** (2009) 1601–1614, [arXiv:0809.3437 \[astro-ph\]](#).
- [41] [www.th.u-psud.fr/NMHDECAY/nmssmtools.html](http://www.th.u-psud.fr/NMHDECAY/nmssmtools.html)
- [42] A. Arbey and F. Mahmoudi, “SuperIso Relic: A program for calculating relic density and flavor physics observables in Supersymmetry,” *Comput.Phys.Commun.* **176** (2007) 367–382, [arXiv:0906.0369 \[hep-ph\]](#).
- [43] G. Belanger, F. Boudjema, A. Pukhov, and A. Semenov, “micrOMEGAs2.0: a program to calculate the relic density of dark matter in a generic model,” *Comput.Phys.Commun.* **181** (2010) 1277–1292, [arXiv:hep-ph/0607059 \[hep-ph\]](#).

- [44] K. L. Chan, U. Chattopadhyay, and P. Nath, “Naturalness, weak scale supersymmetry and the prospect for the observation of supersymmetry at the Tevatron and at the LHC,” *Phys. Rev.* **D58** (1998) 096004, [arXiv:hep-ph/9710473](#). ; J. L. Feng, K. T. Matchev, and T. Moroi, “Focus points and naturalness in supersymmetry,” *Phys. Rev.* **D61** (2000) 075005, [arXiv:hep-ph/9909334](#). ; J. L. Feng, K. T. Matchev, and F. Wilczek, “Neutralino Dark Matter in Focus Point Supersymmetry,” *Phys. Lett.* **B482** (2000) 388–399, [arXiv:hep-ph/0004043](#).
- [45] **LUX Collaboration** Collaboration, D. Akerib *et al.*, “The Large Underground Xenon (LUX) Experiment,” *Nucl.Instrum.Meth.* **A704** (2013) 111–126, [arXiv:1211.3788 \[physics.ins-det\]](#).
- [46] **XENON1T collaboration** Collaboration, E. Aprile, “The XENON1T Dark Matter Search Experiment,” [arXiv:1206.6288 \[astro-ph.IM\]](#).
- [47] S. Bailly, K.-Y. Choi, K. Jedamzik, and L. Roszkowski, “A Re-analysis of Gravitino Dark Matter in the Constrained MSSM,” *JHEP* **0905** (2009) 103, [arXiv:0903.3974 \[hep-ph\]](#). ; L. Roszkowski, S. Trojanowski, K. Turzynski, and K. Jedamzik, “Gravitino dark matter with constraints from Higgs boson mass and sneutrino decays,” *JHEP* **1303** (2013) 013, [arXiv:1212.5587 \[hep-ph\]](#).
- [48] L. Covi, J. E. Kim, and L. Roszkowski, “Axinos as cold dark matter,” *Phys.Rev.Lett.* **82** (1999) 4180–4183, [arXiv:hep-ph/9905212 \[hep-ph\]](#). ; L. Covi, H.-B. Kim, J. E. Kim, and L. Roszkowski, “Axinos as dark matter,” *JHEP* **0105** (2001) 033, [arXiv:hep-ph/0101009 \[hep-ph\]](#). ; K.-Y. Choi, L. Roszkowski, and R. Ruiz de Austri, “Determining reheating temperature at colliders with axino or gravitino dark matter,” *JHEP* **0804** (2008) 016, [arXiv:0710.3349 \[hep-ph\]](#).